

# Global-Local Similarity for Efficient Fine-Grained Image Recognition with Vision Transformers

Edwin Arkel Rios<sup>†</sup>, Min-Chun Hu<sup>‡</sup>, Bo-Cheng Lai<sup>†</sup>

<sup>†</sup>National Yang Ming Chiao Tung University, Taiwan, <sup>‡</sup>National Tsing Hua University, Taiwan

## Abstract

*Fine-grained recognition involves the classification of images from subordinate macro-categories, and it is challenging due to small inter-class differences. To overcome this, most methods perform discriminative feature selection enabled by a feature extraction backbone followed by a high-level feature refinement step. Recently, many studies have shown the potential behind vision transformers as a backbone for fine-grained recognition, but their usage of its attention mechanism to select discriminative tokens can be computationally expensive. In this work, we propose a novel and computationally inexpensive metric to identify discriminative regions in an image. We compare the similarity between the global representation of an image given by the CLS token, a learnable token used by transformers for classification, and the local representation of individual patches. We select the regions with the highest similarity to obtain crops, which are forwarded through the same transformer encoder. Finally, high-level features of the original and cropped representations are further refined together in order to make more robust predictions. Through extensive experimental evaluation we demonstrate the effectiveness of our proposed method, obtaining favorable results in terms of accuracy across a variety of datasets. Furthermore, our method achieves these results at a much lower computational cost compared to the alternatives. Code and checkpoints are available at: <https://github.com/arkel23/GLSim>.*

## 1. Introduction

Fine-grained image recognition (FGIR) involves classifying sub-categories within a larger super-category. Examples of FGIR problems include differentiating between bird species [55, 58] and anime characters [1, 61]. It is a widely studied area with various applications such as automatic biodiversity monitoring, intelligent retail, among others [62]. However, FGIR is a challenging task due to small inter-class differences and large intra-class variations.

In order to tackle these challenges, most of the exist-

ing methods equip a coarse image recognition backbone encoder with modules to select discriminative regions [33, 66]. Recently, with the advent of vision transformers (ViTs) [12], many researchers have explored using this new architecture as a backbone for fine-grained image recognition [18, 59, 71]. Since transformer encoder blocks utilize multi-head self-attention, a natural choice was to use the attention scores to guide the discriminative region selection process, eliminating the need for an external attention module [21, 44, 76]. These regions are either cropped and re-inputted into the same encoder [22, 71], or combined using high-level feature refinement modules [18, 59], or both [24], before making final predictions.

However, as seen in Table 1, several methods leveraging matrix-multiplication for attention aggregation [2, 8, 18, 22, 34, 75] exhibit significant computational expense, characterized by a complexity of  $\mathcal{O}(N^3)$  with respect to the sequence length  $N$ . Notably, the computational cost associated with attention aggregation can exceed that of the backbone’s forward pass, particularly as image size increases. This computational burden presents a substantial limitation for FGIR tasks, which often benefit from the use of higher resolution images [16, 51, 60], thereby constraining the practical applicability of these methods.

To address this, we introduce a novel metric, **GLS (Global-Local Similarity)**, to identify discriminative regions for Vision Transformers (ViTs) with **a computational cost several orders of magnitude lower than that of aggregated attention**. We compute the similarity between the global representation of an image, as given by the ViT’s CLS token typically used for classification, and the local representations of individual patches. Regions exhibiting high similarity in the high-dimensional feature space are presumed to share underlying factors influencing the global representation, rendering them highly representative of the image. We subsequently crop the image based on the regions with highest GLS, resize it, and re-input it into the encoder. Finally, the high-level features of the original and cropped image are refined collectively using an aggregator module, enhancing the robustness of predictions. Our contributions are summarized as follows:

- We propose a novel metric for ViTs to identify discriminative regions in an image. GLS can be used as a visualization tool for interpretability of classification decisions, does not require any additional parameters and exhibits linear complexity  $\mathcal{O}(N)$  with respect to sequence length. Compared to commonly used matrix-multiplication based aggregated attention the computational cost of GLS can be from  $10^3$  up to  $10^6$  times lower, depending on the architecture and image size.
- We incorporate the proposed metric into a method that selects discriminative crops from an image and aggregates high-level features from both the original and cropped image for improved fine-grained image recognition performance.
- We conducted a thorough analysis of fine-grained recognition models by comparing models across 10 datasets spanning a wide spectrum of tasks. Our model achieves the highest accuracy in 8 datasets, and on average, reduces the relative classification error<sup>1</sup> by **10.15%** compared to the baseline ViT. These results demonstrate the potential of the proposed global-local similarity as discriminative region selection criteria. Moreover, our model achieves these results with **9.26x** less VRAM and a **2.59x** higher inference throughput than the best performing model in the other 2 datasets.

## 2. Related Work

### 2.1. Fine-Grained Image Recognition

To address challenges of intra-class variations in FGIR, most approaches aim to identify discriminative regions that encapsulate the subtle differences between classes. Initially, part-level bounding boxes [70] or segmentation masks [63] were employed to train localization subnetworks, but the cost of manual annotations limited their applicability to a wide variety of tasks.

Therefore, researchers aimed to use weak supervision, i.e., image-level labels, to localize discriminative regions. In this category most methods utilize either RPN [46] or attention mechanism for this goal. NTS-Net [66] is an example of the former that leverages classifier confidence to encourage collaboration between a Navigator and a Teacher network to propose and evaluate informative regions. RA-CNN [15], WS-DAN [21] and CAL [44] are examples of the latter approach. RA-CNN employs an attention proposal subnetwork that recursively proposes finer regions, while WS-DAN and CAL use attention maps to generate augmentations of the image. While these methods achieve competitive results, they rely on external (attention) modules that increase the computational cost. Moreover, they

<sup>1</sup>Relative error:  $Err_{rel} = 100 \cdot \frac{(100 - Acc) - (100 - Acc_{ref})}{100 - Acc_{ref}}$

require multiple recursive stages or multiple crops to obtain high-quality predictions, which further exacerbates the computational cost and limits their practicality.

### 2.2. Transformers for Fine-Grained Recognition

Recently, with the emergence of transformers in vision, there has been a substantial amount of research in how to effectively exploit this new architecture for FGIR [18, 22, 59]. The global receptive field of the self-attention mechanism, coupled with the inherent relative importance imparted by the attention weights, makes the ViT a natural candidate for usage as a backbone for fine-grained tasks.

In Table 1 we compare the cost of the discriminative feature selection modules (DFSM) of proposed ViTs for FGIR as we observe it is the largest difference between these methods. All evaluated methods make use of the ViT’s attention mechanism, mostly by leveraging recursive layer-wise matrix-matrix multiplication (TransFG [18], RAMS-Trans [22], DCAL [75], TPSKG [34], EV [8]) to calculate aggregated attention scores. RAMS-Trans and DCAL first compute the mean over different heads, while TransFG computes these scores separately for each head. AFTrans [71] computes head-wise aggregation of attention via element-wise multiplication, and re-weights layer contributions via its Squeeze-and-Excitation-like mechanism. FFVT [59] selects features on a layer-by-layer basis based on the normalized vector product of the first row and column of the attention matrix.

Nevertheless, methods involving matrix-matrix multiplications incur a high computational cost that can even surpass the cost of the backbone itself, specially as the image size increases. The number of FLOPs required for multiplying two matrices  $M_1 \in \mathbb{R}^{N \times N}$  and  $M_2 \in \mathbb{R}^{N \times N}$  is  $N \cdot N \cdot (2N - 1)$ . For TransFG, which entails  $H$  heads, and requires  $L - 2$  multiplications in the process of the PSM, its computational complexity is  $\mathcal{O}(L \cdot H \cdot N^3)$ . Those employing attention rollout [2] such as RAMS-Trans average the heads, thereby reducing the complexity by a factor of  $H$ . Although AF-Trans does not perform matrix-matrix multiplication, it still recursively computes  $N^2$  element-wise products for  $H$  heads in each layer. The computationally lightest DFSM is FFVT’s MAWS since it does not involve large matrix products. However, it exhibits considerable variation in performance across tasks, as observed from the results in Section 5 and poor interpretability as observed from the visualization in Figure 2.

### 2.3. Similarity in Computer Vision

Determining similarity between visual data is a fundamental requirement in various computer vision applications, including image retrieval and matching [11, 48]. Typically, deep feature extraction models are employed to learn a high-level feature space, where metrics such as cosine sim-

Model	TransFG [18]	Various [22, 34, 75]	FFVT [59]	AF-Trans [22]	Ours
DFSM	PSM	Rollout	MAWS	SACM	GLS
Complexity	$L \cdot H \cdot N^3$	$L \cdot N^3$	$L \cdot H \cdot N$	$L \cdot H \cdot N^2$	$N \cdot D$
FLOPs (IS=224)	$8.2 \times 10^3$	$1.7 \times 10^2$	$1.3 \times 10^{-1}$	$1.4 \times 10^1$	$4.5 \times 10^{-1}$
% of Backbone	46.531	0.9833	0.0007	0.0795	0.0026
FLOPs (IS=448)	$6.2 \times 10^5$	$1.1 \times 10^4$	$5.3 \times 10^{-1}$	$2.5 \times 10^2$	$1.8 \times 10^0$
% of Backbone	<b>781.31</b>	13.592	0.0007	0.3162	0.0023
FLOPs (IS=768)	$1.5 \times 10^7$	$2.7 \times 10^5$	$1.5 \times 10^0$	$2.1 \times 10^3$	$5.3 \times 10^0$
% of Backbone	<b>5065.4</b>	<b>91.152</b>	0.0005	0.7072	0.0018
FLOPs (IS=1024)	$9.1 \times 10^7$	$1.5 \times 10^6$	$2.7 \times 10^0$	$6.9 \times 10^3$	$9.4 \times 10^0$
% of Backbone	<b>13674</b>	<b>228.84</b>	0.0004	1.0487	0.0014

Table 1. Summary of computational cost for discriminative feature selection mechanisms (DFSM) used by ViTs in FGIR and their ratio of FLOPs compared to the backbone for ViT B-16. We highlight in **bold** values that exceed 50% of the FLOPs of the backbone.

ilarity, L1, or L2 distance facilitate target retrieval given a query. Examples include CLIP and CCFR. CLIP [43] achieves this by training image and text encoders to optimize cosine similarity for correct image-text pairs and minimize it for incorrect pairs. CCFR [65] leverages cosine similarity to retrieve external features from a database to re-rank fine-grained classification predictions. Our approach, however, is distinct in that it is more closely related to self-similarity [48], computing similarity within a single image rather than against external images.

Self-similarity is commonly used as a descriptor that reveals the structural layout of an image or video by measuring similarities of a local patch within its neighborhood [25, 48]. Recently, self-similarity has been harnessed as an intermediate feature transformation in deep neural networks, demonstrating its efficacy in video understanding [31], image translation [72], visual correspondence [29], few-shot image recognition [26], and image retrieval [32].

While self-similarity typically involves transformations based on local patch neighborhoods, our approach computes similarity between the global image representation and individual patches. As a result, our method deviates from conventional self-similarity, which focuses on local patch relations, and instead employs the similarity between the global representation and local features as a metric for discriminative feature selection.

### 3. Proposed Method: GLSim

An overview of our method is shown in Figure 1. Images are encoded using a transformer encoder. Then, to find discriminative regions, we employ the Global-Local Similarity (GLS) Module. The GLS Module computes the similarity between the global representation of the image and local tokens and crops the image based on the tokens with highest similarity. The image is then resized and forwarded through the encoder. Finally, an Aggregator module is employed to collectively refine high-level features from the original and

cropped image, before being forwarded through a classification head to make our final predictions.

#### 3.1. Image Encoding with Vision Transformer

We encode images using a ViT [12] encoder. Images are patchified using a convolution with large kernel size  $P$  and flattened into a 1D sequence of  $D$  channels and length  $N = (S_1/P) \times (S_2/P)$ , where  $S_1$  and  $S_2$  represent the image width and height. Inspired by BERT [10], the authors concatenate a learnable CLS token at the start of the sequence. Learnable positional embeddings are added to the sequence to incorporate spatial information. This sequence is forwarded through a series of  $L$  transformer encoder blocks [57] which apply multi-head self-attention (MHSA) with  $H$  heads and position-wise feed-forward networks (PWFFN), before being forwarded through a Layer Normalization [3] layer. This output of the transformer is denoted as  $\mathbf{f} \in \mathbb{R}^{(N+1) \times D}$ .

#### 3.2. Discriminative Feature Selection With GLS

To identify the discriminative regions in the image, we then compute the similarity between the global representation of the image, as given by the CLS token ( $\mathbf{f}^0$ ) and each of the other tokens in the sequence. This similarity map, denoted as  $\mathbf{s} \in \mathbb{R}^{N \times D}$ , is calculated according to Equations (1) and (2) when cosine similarity is employed as similarity measure:

$$\mathbf{s}^i = \text{sim}(\mathbf{f}^0, \mathbf{f}^i) = \cos(\mathbf{f}^0, \mathbf{f}^i) \quad i \in 1, 2, \dots, N \quad (1)$$

$$\cos(\mathbf{f}^0, \mathbf{f}^i) = \frac{\mathbf{f}^0 \cdot \mathbf{f}^i}{\|\mathbf{f}^0\| \|\mathbf{f}^i\|} = \frac{\sum_{j=1}^D f_j^0 f_j^i}{\sqrt{\sum_{j=1}^D f_j^0} \sqrt{\sum_{j=1}^D f_j^i}} \quad (2)$$

Then, we crop the image based on the image coordinates corresponding to a rectangle that encloses the top- $O$  tokens

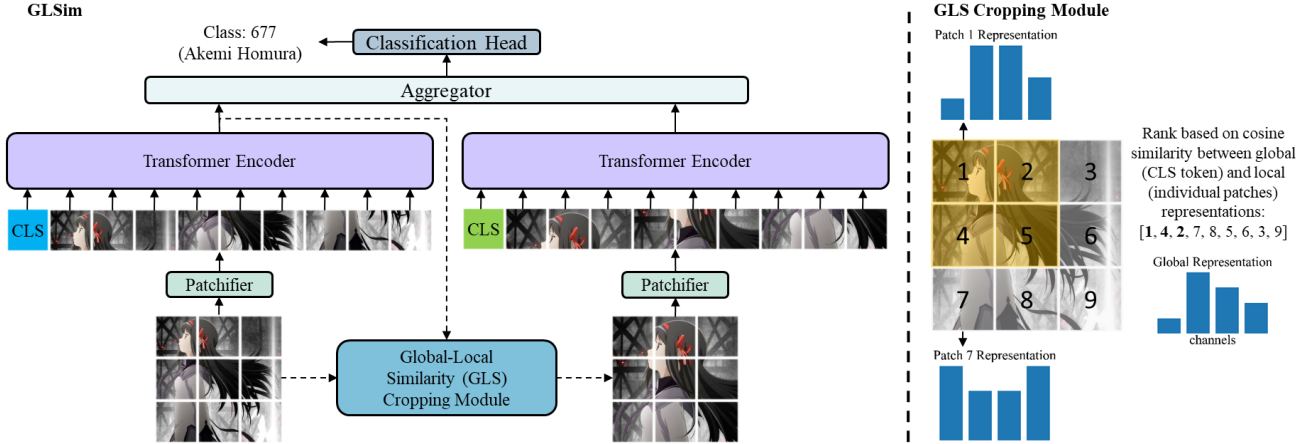


Figure 1. Overall flow of our proposed system, GLSim. Starting from the bottom left corner, an image is patchified and passed through a series of transformer encoder blocks to extract features. These are then used by the GLS Module to select discriminative crops, as indicated by the dashed-lines. The GLS Module crops the image according to the coordinates corresponding to the top- $O$  tokens with the highest similarity between global and local representations of the encoded image. The cropped image is then passed through the same encoder. Finally, high-level features from the original and cropped image are refined using an Aggregator module before making the final predictions.

with highest similarity. Subsequently, the cropped image is resized to the original image size  $S_1 \times S_2$  before being forwarded through the encoder to obtain  $\mathbf{f}_{crops}$ . While the encoder’s weights are shared, a different CLS token is utilized for the crops, drawing inspiration from [22].

As the CLS token aggregates the discriminative details from the image through self-attention, we expect the local tokens with high degree of similarity in the high-dimensional feature space to share the same underlying factors that drive the global representation. To verify our assumptions, we visualize various discriminative feature selection mechanisms (DFSMs) in Figure 2. We note that single-layer attention [59], as depicted in the second and third column of the figure, does not focus on the objects of interest in certain scenarios. Conversely, while aggregating multiple layers attention through recursive matrix multiplication (fourth and fifth column) may offer a more effective alternative, it comes at a significant computational cost, up to 13,674x and 229x higher than the forward pass of the backbone, as seen in Table 1. On the other side, while heatmaps of global-local similarity (last column) may not exhibit the same level of focus on specific regions as the aggregated attention maps, they are still mostly aligned with the regions of interest and the computational cost is much lower as seen in Table 1. In particular, GLS requires between  $10^3$  to  $10^7$  times **less FLOPs** compared to attention rollout [2] and TransFG’s PSM [18], making it a highly efficient and effective alternative to attention.

### 3.3. High-Level Feature Refinement

In order to achieve more robust predictions, we explicitly combine high-level features from both the original and cropped images by incorporating an Aggregator module comprised of a single transformer encoder block. Specifically, we concatenate the output CLS token of the original image ( $\mathbf{f}^0$ ) and the cropped image ( $\mathbf{f}_{crops}^0$ ), and forward this concatenated representation through the Aggregator module. This is shown in Equations (3) and (4):

$$\mathbf{r}' = \text{MHSA}(\text{LN}([\mathbf{f}^0; \mathbf{f}_{crops}^0]) + [\mathbf{f}^0; \mathbf{f}_{crops}^0]). \quad (3)$$

$$\mathbf{r} = \text{PWFFN}(\text{LN}(\mathbf{r}') + \mathbf{r}') \quad (4)$$

Then we pass these tokens through a LayerNorm layer. We forward the first token in the sequence through a linear layer  $C_{final} \in \mathbb{R}^{D \times T}$  to obtain our final classification predictions. We utilize cross-entropy as our loss function. This process is described by Equations (5) and (6):

$$\mathbf{r}_{LN} = \text{LN}(\mathbf{r}) \quad (5)$$

$$y_{final} = \mathbf{r}_{LN}^0 C_{final} \quad (6)$$

## 4. Datasets and Experimental Setup

We conduct experiments on 10 datasets, whose detailed statistics are shown in the Appendix. We perform a learning rate (LR) search for each dataset-model pair with a small split from the train set. Then as suggested by Gwilliam et al. [17] we report mean accuracy and its standard deviation on the test set across different seeded runs. The best

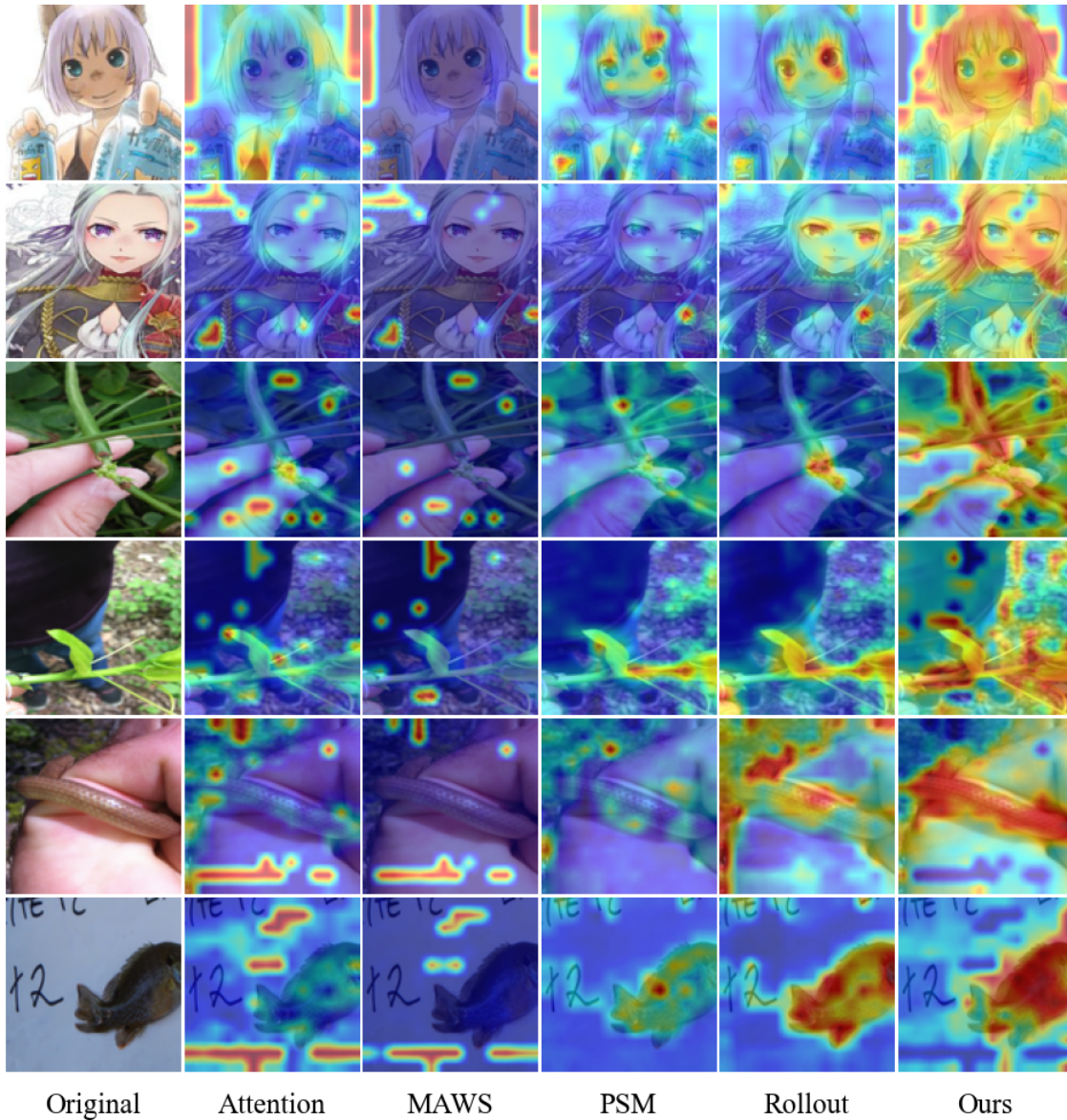


Figure 2. Visualization of discriminative feature selection mechanisms for a fine-tuned ViT B-16 on DAFB [7, 47] (first 2 rows) and iNat17 [56] (last 4 rows) dataset. From left to right: original image, head-wise average of attention scores of last layer, MAWS [59] of last layer, PSM [18], attention rollout [2], and our proposed global-local similarity.

and second best results, when applicable, are highlighted by **boldface** and underline, respectively.

We employ the ViT B-16 [12] pre-trained on ImageNet-21k as the backbone for our proposed model. The hyperparameter  $O$ , which determines how many tokens with highest similarity we use for cropping, is set to 8 for most datasets, except for Dogs where it is set to 16. This value is doubled accordingly when using image size 448. We compare our proposal against several existing state-of-the-art

(SotA) models, including the baseline ViT, two other ViTs specifically designed for FGIR (namely, TransFG [18] and FFVT [59]), as well as two CNN-based approaches, namely ResNet-101 [19], and CAL [44] which employs the former as a backbone. The source code provided by the authors was incorporated into our training and evaluation codebase with minor modifications.

We resize images to a square of size  $1.34S_1 \times 1.34S_2$  (e.g., 300x300 for image size 224x224) then perform a

random crop during training or a center crop at inference. During training we additionally apply random horizontal flipping, random erasing [74], trivial augment [38], label smoothing [52] and stochastic depth [23].

We employ the SGD optimizer with batch size of 8, weight decay of 0 and cosine annealing [35] with a warmup of 500 steps for learning rate scheduling. Models are trained for 50 epochs. We use PyTorch [42] with mixed precision and employ Weight and Biases [5] for logging and experiment tracking. We conduct all experiments using a single V100 GPU.

## 5. Results and Discussion

### 5.1. FGIR SotA Model Comparison

#### 5.1.1 Comparison on NABirds

In the NABirds [55] dataset the accuracies of most ViT-based methods are higher compared to CNN-based methods. This could be due to the usage of the self-attention operator with its global receptive field which can allow for effective aggregation of discriminative features from diverse regions of the image. Our method outperforms the best CNN-based method by 1%. Compared to ViT-based methods, our method outperforms the baseline ViT by 3.1%, while the second best, Dual-TR [24] by 0.7%.

Method	Backbone	Top-1 (%)
MaxEnt [14]	DenseNet-161	83.0
Cross-X [36]	ResNet-50	86.4
API-Net [76]	ResNet-101	88.1
CS-Parts [30]	ResNet-50	88.5
MGE-CNN [69]	ResNet-101	88.6
CAP [4]	Xception	91.0
ViT B-16 [12]	ViT B-16	89.9
DeiT B-16 [53]	DeiT B-16	87.3
TPSKG [34]	ViT B-16	90.1
TransFG [18]	ViT B-16	90.8
IELT [64]	ViT B-16	90.8
Dual-TR [24]	ViT B-16	<u>91.3</u>
R2-Trans [68]	ViT B-16	90.2
DeiT-NeT [28]	DeiT B-16	88.4
GLSim (Ours)	ViT B-16	<b>92.0</b>

Table 2. Recognition accuracy for state-of-the-art models on NABirds [55] dataset with image size 448x448.

#### 5.1.2 Comparison on iNat17

In the challenging iNat17 [56], our method attains an improvement of 1.5% compared to the second best performing method, DeiT-NeT [28] which employs a ViT trained

with the DeiT [53] pretraining recipe. Among models using the ViT B-16 pretraining recipe, our model outperforms the next best, TransFG [18] by 3.8% absolute accuracy, while the baseline ViT by 6.8%. This increase in relative improvement on the iNat17 dataset shows the promise behind our proposed methodology for large-scale FGIR tasks.

Method	Backbone	Top-1 (%)
ResNet-152 [19]	ResNet-152	59.0
SpineNet-143 [13]	SpineNet-143	63.6
IncResNetV2 SE [56]	IncResNetV2	67.3
SSN [45]	ResNet-101	65.2
TASN [73]	ResNet-101	68.2
ViT B-16 [12]	ViT B-16	68.7
DeiT B-16 [53]	DeiT B-16	72.8
RAMS-Trans [22]	ViT B-16	68.5
AFTrans [71]	ViT B-16	68.9
SIM-Trans [50]	ViT B-16	69.9
TransFG [18]	ViT B-16	71.7
Dual-TR [24]	ViT B-16	71.5
DeiT-NeT [28]	DeiT B-16	<u>74.0</u>
GLSim (Ours)	ViT B-16	<b>75.5</b>

Table 3. Recognition accuracy for state-of-the-art models on iNat17 [56] dataset with image size 304x304.

#### 5.1.3 Comparison Using Image Size 224x224

Previous research suggested the applicability of FGIR methods is task dependent [67]. Therefore, to obtain a better understanding of how our method performs across FGIR tasks we conduct a comparison across 10 FGIR datasets using image size 224x224 in Table 4. Our proposed method, GLSim, obtains the highest accuracy in 8 datasets (CUB, Dogs, Flowers, Food, iNat17, NABirds, Pets, VegFru) and the second best in 2 others (DAFB, Moe). On average our method obtains the highest classification accuracy, reducing the relative classification error by 10.15% compared to the baseline ViT. These results demonstrate the robustness of GLSim across a wide variety of FGIR domains.

## 5.2. Qualitative evaluation

We evaluate the relation of the proposed global-local similarity to the quality of our crops and also compare them to crops from CAL by visualizing samples from various fine-grained datasets in Figure 3. In general, our method adeptly capture the objects of interest present within the corresponding images, thereby mitigating the impact of background noise. This, in turns, facilitates the extraction of finer details during the second forward pass.

When comparing our cropping method to CAL on the DAFB dataset, we observe that our approach yields more

Dataset	CNN-Based		ViT-Based			
	RN-101 [19]	CAL [44]	ViT B-16 [12]	TransFG [18]	FFVT [59]	Ours
CUB [58]	82.71 ± 0.06	88.44 ± 0.25	90.11 ± 0.17	<u>90.49 ± 0.06</u>	90.05 ± 0.04	<b>90.93 ± 0.24</b>
DAFB [7]	91.20 ± 0.08	<b>95.15 ± 0.01</b>	91.78 ± 0.06	92.87 ± 0.01	91.49 ± 0.01	<u>93.36 ± 0.02</u>
Dogs [27]	91.10 ± 0.18	89.78 ± 0.10	91.36 ± 0.05	90.68 ± 0.14	<u>91.49 ± 0.01</u>	<b>92.01 ± 0.09</b>
Flowers [39]	92.36 ± 0.24	98.14 ± 0.04	<u>99.45 ± 0.03</u>	99.44 ± 0.03	99.32 ± 0.02	<b>99.48 ± 0.02</b>
Food [6]	87.45 ± 0.21	89.71 ± 0.12	92.43 ± 0.04	<u>92.76 ± 0.05</u>	91.89 ± 0.01	<b>92.97 ± 0.04</b>
iNat17 [56]	63.37 ± 0.16	69.29 ± 0.03	69.38 ± 0.04	<u>72.34 ± 0.12</u>	69.09 ± 0.04	<b>73.50 ± 0.06</b>
Moe [1]	94.22 ± 0.06	<b>97.55 ± 0.00</b>	96.47 ± 0.11	96.59 ± 0.20	<u>96.67 ± 0.15</u>	<b>96.67 ± 0.16</b>
NABirds [55]	81.00 ± 0.26	88.33 ± 0.49	87.36 ± 0.09	<u>88.76 ± 0.08</u>	86.63 ± 0.08	<b>89.11 ± 0.16</b>
Pets [41]	93.20 ± 0.19	93.89 ± 0.23	94.10 ± 0.07	<u>93.93 ± 0.14</u>	<u>94.34 ± 0.11</u>	<b>95.01 ± 0.18</b>
VegFru [20]	89.34 ± 0.05	90.33 ± 4.28	95.77 ± 0.05	<u>95.91 ± 0.04</u>	<u>95.58 ± 0.02</u>	<b>96.14 ± 0.04</b>
Average	86.59 ± 9.25	90.06 ± 8.16	90.84 ± 8.29	<u>91.38 ± 7.41</u>	90.56 ± 8.39	<b>91.92 ± 7.14</b>

Table 4. Recognition accuracy for state-of-the-art models with image size 224x224.

zoomed-in crops than those produced by CAL. This tighter cropping may inadvertently exclude critical details necessary for effective discrimination in this task. Additionally, CAL’s use of multiple crops could account for the observed accuracy gap between our method and CAL.

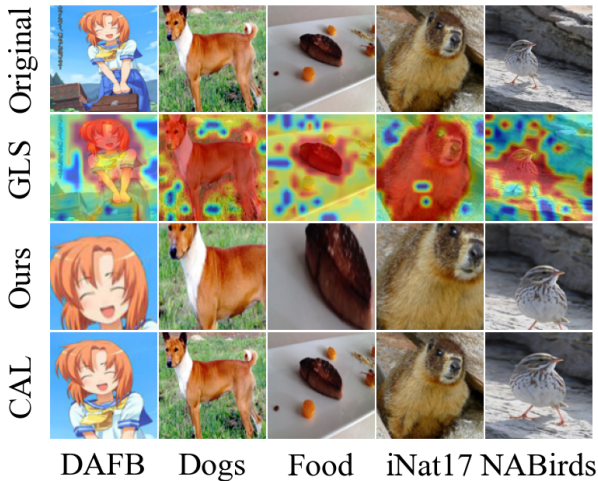


Figure 3. Visualization of samples from various fine-grained datasets. First row shows the original images. Second and third rows show the heatmap for the proposed global-local similarity (GLS) metric and crops obtained based on it. Fourth row shows crops for CAL [44].

### 5.3. Computational Cost Analysis

As the accuracy of FGIR models reaches a certain threshold, the computational cost of deploying them becomes a critical factor. We compare the trade-off between accuracy and the throughput (in images per second) at inference time when batching the images, and the associated VRAM required for computing this batched inference.

We show the results on Figure 4 on accuracy vs inference throughput as for many users the throughput is a limiting factor when deploying models with real-time requirements. From this figure, we can observe that GLSim with image size 224 obtains a competitive accuracy, that is only surpassed by ViT, TransFG, FFVT and GLSim with image size 448, albeit slightly. However, the throughput for GLSim with image size 224 is 2.70x, 8.73x, 4.00x, and 5.11x times higher compared to the aforementioned models with image size 448.

With regards to VRAM, we highlight the low memory requirements of GLSim with image size 224 as it is the only model to require less than 1 GB of VRAM during inference. This is because unlike TransFG and FFVT it does not require the storage and processing of intermediate features. GLSim requires 5.45x and 5.29x less VRAM compared to TransFG, and 2.32x and 1.65x less VRAM compared to FFVT, for image sizes 224 and 448, respectively.

Furthermore, when compared to CAL, which yields the best results in DAFB and Moe, our proposed method has higher throughput, and requires substantially less VRAM during inference. Specifically, our method has 2.59x and 1.48x higher throughput, and requires 9.26x and 8.11x less VRAM, for image size 224 and 448, respectively.

Overall, these results suggest that our proposed method achieves high accuracy while keeping computational cost low, making it a practical and efficient solution for deploying FGIR models in real-world applications.

### 5.4. Ablation on Proposed Components

We present a breakdown of the individual contributions of the proposed components of our system in Table 5. The first row outlines the performance of the baseline ViT B-16 model, while the second row reflects the outcomes of a modified ViT with an extra encoder block that only processes the CLS token. The third row describes a scenario

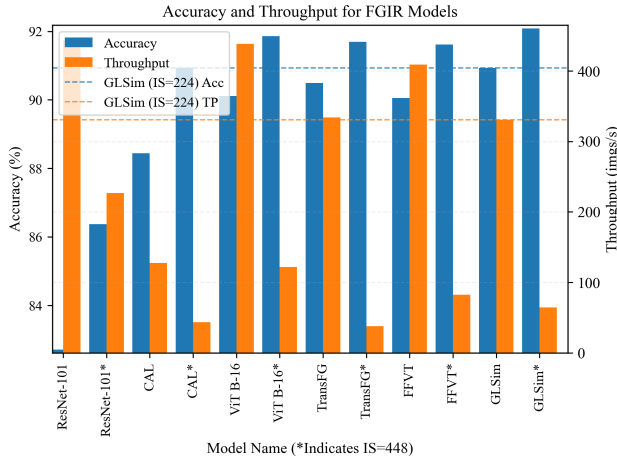


Figure 4. Accuracy and throughput plots for the evaluated models on CUB. *Model\** represents results for image size 448x448. We highlight the accuracy and throughput for our proposed GLSim method with image size 224x224.

where we select and encode image crops but do not explicitly combine high-level features. Instead, we choose the prediction with the highest confidence between the original image and the cropped image. Finally, the fourth row represents our complete system, GLSim.

The proposed Aggregator and GLS Cropping modules reduce the relative classification error by 4.41% and 4.38%, respectively. By incorporating both modules the error is further reduced by an additional 4.12% compared to cropping without explicit high-level feature aggregation. This highlights the importance of the proposed modules to the overall effectiveness of our system.

GLS	Aggregator	Accuracy (%)
-	-	90.11 ± 0.17
-	✓	90.55 ± 0.06
✓	-	90.54 ± 0.16
✓	✓	<b>90.93 ± 0.24</b>

Table 5. Ablation on proposed components on CUB.

## 6. Future Work: GLS For Visualization and Downstream Tasks

The proposed GLS metric can be used as a visualization tool to highlight which local regions of the image have high similarity to the global representation from the CLS token to interpret classification predictions. Furthermore, GLS shows even better discrimination performance when combined with state-of-the-art pretrained backbones such

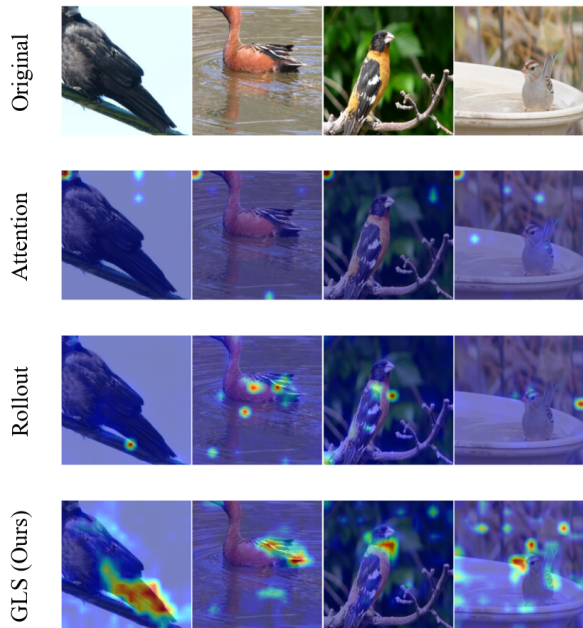


Figure 5. Visualization of attention-based visualization mechanisms and our proposed GLS for DINOv2 B-14 [40] on NABirds.

as DINOv2 [40] as shown in Figure 5. This could allow deploying these models in a variety of downstream tasks such as fine-grained weakly supervised localization and semantic segmentation [37, 49], fine-grained object recognition based on remote sensing imagery [16, 51, 60] where resources are constrained. We remark how the computational cost of our proposed GLS can range from **648x to 271,299x less** compared to matrix-multiplication based attention aggregation mechanisms [8, 18, 22, 34, 75], for a B-14 backbone with image size ranging from 224 to 1024.

## 7. Conclusion

This paper proposes GLS, an efficient and effective alternative to attention scores in vision transformers, for the purpose of discriminative region identification to enhance fine-grained image recognition. GLS compares the similarity between global and local representations of an image. Based on this we propose a system GLSim which extracts discriminative crops and combines high-level features from both the original and cropped image using an aggregator module for robust predictions. Extensive evaluations across various datasets demonstrate the robustness of our method.

## References

- [1] Tagged Anime Illustrations. 1, 7, 15

- [2] Samira Abnar and Willem Zuidema. Quantifying Attention Flow in Transformers, May 2020. arXiv:2005.00928 [cs]. 1, 2, 4, 5
- [3] Jimmy Lei Ba, Jamie Ryan Kiros, and Geoffrey E. Hinton. Layer Normalization. 2016. Publisher: arXiv Version Number: 1. 3
- [4] Ardendu Behera, Zachary Wharton, Pradeep R. P. G. Hewage, and Asish Bera. Context-aware Attentional Pooling (CAP) for Fine-grained Visual Classification. *Proceedings of the AAAI Conference on Artificial Intelligence*, 35(2):929–937, May 2021. Number: 2. 6
- [5] Lukas Biewald. Experiment Tracking with Weights and Biases, 2020. 6
- [6] Lukas Bossard, Matthieu Guillaumin, and Luc Van Gool. Food-101 – Mining Discriminative Components with Random Forests. In David Fleet, Tomas Pajdla, Bernt Schiele, and Tinne Tuytelaars, editors, *Computer Vision – ECCV 2014*, Lecture Notes in Computer Science, pages 446–461, Cham, 2014. Springer International Publishing. 7, 15
- [7] Gwern Branwen. Danbooru2021: A Large-Scale Crowdsourced and Tagged Anime Illustration Dataset. Dec. 2015. 5, 7, 15
- [8] Marcos V. Conde and Kerem Turgutlu. Exploring Vision Transformers for Fine-grained Classification, June 2021. arXiv:2106.10587 [cs]. 1, 2, 8
- [9] Ekin D. Cubuk, Barret Zoph, Dandelion Mane, Vijay Vasudevan, and Quoc V. Le. AutoAugment: Learning Augmentation Policies from Data, Apr. 2019. arXiv:1805.09501 [cs, stat]. 15
- [10] Jacob Devlin, Ming-Wei Chang, Kenton Lee, and Kristina Toutanova. BERT: Pre-training of Deep Bidirectional Transformers for Language Understanding. *arXiv:1810.04805 [cs]*, May 2019. arXiv: 1810.04805. 3
- [11] Haiwen Diao, Ying Zhang, Lin Ma, and Huchuan Lu. Similarity Reasoning and Filtration for Image-Text Matching. *Proceedings of the AAAI Conference on Artificial Intelligence*, 35(2):1218–1226, May 2021. Number: 2. 2
- [12] Alexey Dosovitskiy, Lucas Beyer, Alexander Kolesnikov, Dirk Weissenborn, Xiaohua Zhai, Thomas Unterthiner, Mostafa Dehghani, Matthias Minderer, Georg Heigold, Sylvain Gelly, Jakob Uszkoreit, and Neil Houlsby. An Image is Worth 16x16 Words: Transformers for Image Recognition at Scale. *arXiv:2010.11929 [cs]*, Oct. 2020. arXiv: 2010.11929. 1, 3, 5, 6, 7, 15
- [13] Xianzhi Du, Tsung-Yi Lin, Pengchong Jin, Golnaz Ghiasi, Mingxing Tan, Yin Cui, Quoc V. Le, and Xiaodan Song. SpineNet: Learning Scale-Permuted Backbone for Recognition and Localization. In *2020 IEEE/CVF Conference on Computer Vision and Pattern Recognition (CVPR)*, pages 11589–11598, Seattle, WA, USA, June 2020. IEEE. 6
- [14] Abhimanyu Dubey, Otkrist Gupta, Ramesh Raskar, and Nikhil Naik. Maximum-Entropy Fine Grained Classification. In *Advances in Neural Information Processing Systems*, volume 31. Curran Associates, Inc., 2018. 6
- [15] Jianlong Fu, Heliang Zheng, and Tao Mei. Look Closer to See Better: Recurrent Attention Convolutional Neural Network for Fine-Grained Image Recognition. In *2017 IEEE Conference on Computer Vision and Pattern Recognition (CVPR)*, pages 4476–4484, July 2017. ISSN: 1063-6919. 2
- [16] Bo Guo, Ruixiang Zhang, Haowen Guo, Wen Yang, Huai Yu, Peng Zhang, and Tongyuan Zou. Fine-Grained Ship Detection in High-Resolution Satellite Images With Shape-Aware Feature Learning. *IEEE Journal of Selected Topics in Applied Earth Observations and Remote Sensing*, 16:1914–1926, 2023. Conference Name: IEEE Journal of Selected Topics in Applied Earth Observations and Remote Sensing. 1, 8
- [17] Matthew Gwilliam, Adam Teuscher, Connor Anderson, and Ryan Farrell. Fair Comparison: Quantifying Variance in Results for Fine-Grained Visual Categorization. pages 3309–3318, 2021. 4
- [18] Ju He, Jie-Neng Chen, Shuai Liu, Adam Kortylewski, Cheng Yang, Yutong Bai, and Changhu Wang. TransFG: A Transformer Architecture for Fine-Grained Recognition. In *Proceedings of the First MiniCon Conference*, Feb. 2022. 1, 2, 3, 4, 5, 6, 7, 8, 14, 15, 16
- [19] Kaiming He, Xiangyu Zhang, Shaoqing Ren, and Jian Sun. Deep Residual Learning for Image Recognition. *arXiv:1512.03385 [cs]*, Dec. 2015. arXiv: 1512.03385. 5, 6, 7, 15
- [20] Saihui Hou, Yushan Feng, and Zilei Wang. VegFru: A Domain-Specific Dataset for Fine-Grained Visual Categorization. pages 541–549, 2017. 7, 15
- [21] Tao Hu, Honggang Qi, Qingming Huang, and Yan Lu. See Better Before Looking Closer: Weakly Supervised Data Augmentation Network for Fine-Grained Visual Classification, Mar. 2019. arXiv:1901.09891 [cs]. 1, 2, 15, 16
- [22] Yunqing Hu, Xuan Jin, Yin Zhang, Haiwen Hong, Jingfeng Zhang, Yuan He, and Hui Xue. RAMS-Trans: Recurrent Attention Multi-scale Transformer for Fine-grained Image Recognition. In *Proceedings of the 29th ACM International Conference on Multimedia*, MM ’21, pages 4239–4248, New York, NY, USA, Oct. 2021. Association for Computing Machinery. 1, 2, 3, 4, 6, 8, 14
- [23] Gao Huang, Yu Sun, Zhuang Liu, Daniel Sedra, and Kilian Q. Weinberger. Deep Networks with Stochastic Depth. In Bastian Leibe, Jiri Matas, Nicu Sebe, and Max Welling, editors, *Computer Vision – ECCV 2016*, Lecture Notes in Computer Science, pages 646–661, Cham, 2016. Springer International Publishing. 6, 14, 15
- [24] Ruyi Ji, Jiaying Li, Libo Zhang, Jing Liu, and Yanjun Wu. Dual Transformer With Multi-Grained Assembly for Fine-Grained Visual Classification. *IEEE Transactions on Circuits and Systems for Video Technology*, 33(9):5009–5021, Sept. 2023. Conference Name: IEEE Transactions on Circuits and Systems for Video Technology. 1, 6
- [25] Imran N. Junejo, Emilie Dexter, Ivan Laptev, and Patrick Pérez. Cross-View Action Recognition from Temporal Self-similarities. In David Forsyth, Philip Torr, and Andrew Zisserman, editors, *Computer Vision – ECCV 2008*, Lecture Notes in Computer Science, pages 293–306, Berlin, Heidelberg, 2008. Springer. 3
- [26] Dahyun Kang, Heeseung Kwon, Juhong Min, and Minsu Cho. Relational Embedding for Few-Shot Classification. In

- 2021 *IEEE/CVF International Conference on Computer Vision (ICCV)*, pages 8802–8813, Montreal, QC, Canada, Oct. 2021. IEEE. 3
- [27] Aditya Khosla, Nityananda Jayadevaprakash, Bangpeng Yao, and Li Fei-Fei. Novel Dataset for Fine-Grained Image Categorization. In *First Workshop on Fine-Grained Visual Categorization, IEEE Conference on Computer Vision and Pattern Recognition*, Colorado Springs, CO, June 2011. 7, 15
- [28] Sangwon Kim and Byoung Chul Ko. Neural Tree Decoder for Interpretation of Vision Transformers. *IEEE Transactions on Artificial Intelligence*, 5(5):2067–2078, May 2024. Conference Name: IEEE Transactions on Artificial Intelligence. 6
- [29] Seungryong Kim, Dongbo Min, Bumsu Ham, Stephen Lin, and Kwanghoon Sohn. FCSS: Fully Convolutional Self-Similarity for Dense Semantic Correspondence. *IEEE Transactions on Pattern Analysis and Machine Intelligence*, 41(3):581–595, Mar. 2019. Conference Name: IEEE Transactions on Pattern Analysis and Machine Intelligence. 3
- [30] Dimitri Korsch, Paul Bodesheim, and Joachim Denzler. Classification-Specific Parts for Improving Fine-Grained Visual Categorization. In Gernot A. Fink, Simone Frintrap, and Xiaoyi Jiang, editors, *Pattern Recognition*, pages 62–75, Cham, 2019. Springer International Publishing. 6
- [31] Heeseung Kwon, Manjin Kim, Suha Kwak, and Minsu Cho. Learning Self-Similarity in Space and Time as Generalized Motion for Video Action Recognition, Nov. 2021. arXiv:2102.07092 [cs]. 3
- [32] Seongwon Lee, Suhyeon Lee, Hongje Seong, and Euntai Kim. Revisiting Self-Similarity: Structural Embedding for Image Retrieval. pages 23412–23421, 2023. 3
- [33] Chuanbin Liu, Hongtao Xie, Zheng-Jun Zha, Lingfeng Ma, Lingyun Yu, and Yongdong Zhang. Filtration and Distillation: Enhancing Region Attention for Fine-Grained Visual Categorization. *Proceedings of the AAAI Conference on Artificial Intelligence*, 34(07):11555–11562, Apr. 2020. Number: 07. 1
- [34] Xinda Liu, Lili Wang, and Xiaoguang Han. Transformer with peak suppression and knowledge guidance for fine-grained image recognition. *Neurocomputing*, 492:137–149, July 2022. 1, 2, 3, 6, 8, 14
- [35] Ilya Loshchilov and Frank Hutter. SGDR: Stochastic Gradient Descent with Warm Restarts, May 2017. arXiv:1608.03983 [cs, math] version: 5. 6, 13
- [36] Wei Luo, Xitong Yang, Xianjie Mo, Yuheng Lu, Larry S. Davis, Jun Li, Jian Yang, and Ser-Nam Lim. Cross-X Learning for Fine-Grained Visual Categorization. pages 8242–8251, 2019. 6
- [37] Kai A. Metzger, Peter Mortimer, and Hans-Joachim Wuenche. A Fine-Grained Dataset and its Efficient Semantic Segmentation for Unstructured Driving Scenarios. In *2020 25th International Conference on Pattern Recognition (ICPR)*, pages 7892–7899, Jan. 2021. ISSN: 1051-4651. 8
- [38] Samuel G. Müller and Frank Hutter. TrivialAugment: Tuning-free Yet State-of-the-Art Data Augmentation, Aug. 2021. arXiv:2103.10158 [cs]. 6, 14, 15
- [39] Maria-Elena Nilsback and Andrew Zisserman. Automated Flower Classification over a Large Number of Classes. In *2008 Sixth Indian Conference on Computer Vision, Graphics & Image Processing*, pages 722–729, Dec. 2008. 7, 15
- [40] Maxime Oquab, Timothée Darcet, Théo Moutakanni, Huy V. Vo, Marc Szafraniec, Vasil Khalidov, Pierre Fernandez, Daniel Haziza, Francisco Massa, Alaaeldin El-Nouby, Mido Assran, Nicolas Ballas, Wojciech Galuba, Russell Howes, Po-Yao Huang, Shang-Wen Li, Ishan Misra, Michael Rabat, Vasu Sharma, Gabriel Synnaeve, Hu Xu, Herve Jegou, Julien Mairal, Patrick Labatut, Armand Joulin, and Piotr Bojanowski. DINOv2: Learning Robust Visual Features without Supervision. *Transactions on Machine Learning Research*, July 2023. 8, 17, 18, 19, 20, 21
- [41] Omkar M Parkhi, Andrea Vedaldi, Andrew Zisserman, and C. V. Jawahar. Cats and dogs. In *2012 IEEE Conference on Computer Vision and Pattern Recognition*, pages 3498–3505, June 2012. ISSN: 1063-6919. 7, 15
- [42] Adam Paszke, Sam Gross, Francisco Massa, Adam Lerer, James Bradbury, Gregory Chanan, Trevor Killeen, Zeming Lin, Natalia Gimelshein, Luca Antiga, Alban Desmaison, Andreas Kopf, Edward Yang, Zachary DeVito, Martin Raison, Alykhan Tejani, Sasank Chilamkurthy, Benoit Steiner, Lu Fang, Junjie Bai, and Soumith Chintala. PyTorch: An Imperative Style, High-Performance Deep Learning Library. In H. Wallach, H. Larochelle, A. Beygelzimer, F. d’Alché-Buc, E. Fox, and R. Garnett, editors, *Advances in Neural Information Processing Systems 32*, pages 8024–8035. Curran Associates, Inc., 2019. 6
- [43] Alec Radford, Jong Wook Kim, Chris Hallacy, Aditya Ramesh, Gabriel Goh, Sandhini Agarwal, Girish Sastry, Amanda Askell, Pamela Mishkin, Jack Clark, Gretchen Krueger, and Ilya Sutskever. Learning Transferable Visual Models From Natural Language Supervision, Feb. 2021. arXiv:2103.00020 [cs]. 3
- [44] Yongming Rao, Guangyi Chen, Jiwen Lu, and Jie Zhou. Counterfactual Attention Learning for Fine-Grained Visual Categorization and Re-Identification. pages 1025–1034, 2021. 1, 2, 5, 7, 15, 16
- [45] Adrià Recasens, Petr Kellnhofer, Simon Stent, Wojciech Matusik, and Antonio Torralba. Learning to Zoom: A Saliency-Based Sampling Layer for Neural Networks. In Vittorio Ferrari, Martial Hebert, Cristian Sminchisescu, and Yair Weiss, editors, *Computer Vision – ECCV 2018*, volume 11213, pages 52–67. Springer International Publishing, Cham, 2018. Series Title: Lecture Notes in Computer Science. 6
- [46] Shaoqing Ren, Kaiming He, Ross Girshick, and Jian Sun. Faster R-CNN: Towards Real-Time Object Detection with Region Proposal Networks. In *Advances in Neural Information Processing Systems*, volume 28. Curran Associates, Inc., 2015. 2
- [47] Edwin Arkel Rios, Min-Chun Hu, and Bo-Cheng Lai. Anime Character Recognition using Intermediate Features Aggregation. In *2022 IEEE International Symposium on Circuits and Systems (ISCAS)*, pages 424–428, May 2022. ISSN: 2158-1525. 5, 15

- [48] Eli Shechtman and Michal Irani. Matching Local Self-Similarities across Images and Videos. In *2007 IEEE Conference on Computer Vision and Pattern Recognition*, pages 1–8, Minneapolis, MN, USA, June 2007. IEEE. [2](#), [3](#)
- [49] Junghyo Sohn, Eunjin Jeon, Wonsik Jung, Eunsong Kang, and Heung-II Suk. Fine-Grained Attention for Weakly Supervised Object Localization, Apr. 2021. arXiv:2104.04952 [cs]. [8](#)
- [50] Hongbo Sun, Xiangteng He, and Yuxin Peng. SIM-Trans: Structure Information Modeling Transformer for Fine-grained Visual Categorization. In *Proceedings of the 30th ACM International Conference on Multimedia*, MM '22, pages 5853–5861, New York, NY, USA, Oct. 2022. Association for Computing Machinery. [6](#)
- [51] Xian Sun, Peijin Wang, Zhiyuan Yan, Feng Xu, Ruiping Wang, Wenhui Diao, Jin Chen, Jihao Li, Yingchao Feng, Tao Xu, Martin Weinmann, Stefan Hinz, Cheng Wang, and Kun Fu. FAIR1M: A benchmark dataset for fine-grained object recognition in high-resolution remote sensing imagery. *ISPRS Journal of Photogrammetry and Remote Sensing*, 184:116–130, Feb. 2022. [1](#), [8](#)
- [52] Christian Szegedy, Vincent Vanhoucke, Sergey Ioffe, Jon Shlens, and Zbigniew Wojna. Rethinking the Inception Architecture for Computer Vision. In *2016 IEEE Conference on Computer Vision and Pattern Recognition (CVPR)*, pages 2818–2826, June 2016. ISSN: 1063-6919. [6](#), [14](#), [15](#)
- [53] Hugo Touvron, Matthieu Cord, Matthijs Douze, Francisco Massa, Alexandre Sablayrolles, and Hervé Jégou. Training data-efficient image transformers & distillation through attention. *arXiv:2012.12877 [cs]*, Jan. 2021. arXiv: 2012.12877. [6](#), [14](#)
- [54] Hugo Touvron, Matthieu Cord, and Hervé Jégou. DeiT III: Revenge of the ViT, Apr. 2022. arXiv:2204.07118 [cs]. [14](#)
- [55] Grant Van Horn, Steve Branson, Ryan Farrell, Scott Haber, Jessie Barry, Panos Ipeirotis, Pietro Perona, and Serge Belongie. Building a Bird Recognition App and Large Scale Dataset With Citizen Scientists: The Fine Print in Fine-Grained Dataset Collection. pages 595–604, 2015. [1](#), [6](#), [7](#), [15](#)
- [56] Grant Van Horn, Oisin Mac Aodha, Yang Song, Yin Cui, Chen Sun, Alex Shepard, Hartwig Adam, Pietro Perona, and Serge Belongie. The iNaturalist Species Classification and Detection Dataset, Apr. 2018. arXiv:1707.06642 [cs] version: 2. [5](#), [6](#), [7](#), [15](#)
- [57] Ashish Vaswani, Noam Shazeer, Niki Parmar, Jakob Uszkoreit, Llion Jones, Aidan N Gomez, Łukasz Kaiser, and Illia Polosukhin. Attention is All you Need. In *Advances in Neural Information Processing Systems*, volume 30. Curran Associates, Inc., 2017. [3](#)
- [58] Catherine Wah, Steve Branson, Peter Welinder, Pietro Perona, and Serge Belongie. The Caltech-UCSD Birds-200-2011 Dataset. page 8. [1](#), [7](#), [15](#)
- [59] Jun Wang, Xiaohan Yu, and Yongsheng Gao. Feature Fusion Vision Transformer for Fine-Grained Visual Categorization. In *British Machine Vision Conference (BMVC)*, July 2021. arXiv: 2107.02341. [1](#), [2](#), [3](#), [4](#), [5](#), [7](#), [14](#), [15](#), [16](#)
- [60] Liuqian Wang, Jing Zhang, Jimiao Tian, Jiafeng Li, Li Zhuo, and Qi Tian. Efficient Fine-Grained Object Recognition in High-Resolution Remote Sensing Images From Knowledge Distillation to Filter Grafting. *IEEE Transactions on Geoscience and Remote Sensing*, 61:1–16, 2023. Conference Name: IEEE Transactions on Geoscience and Remote Sensing. [1](#), [8](#)
- [61] Yan Wang. Danbooru 2018 Anime Character Recognition Dataset, July 2019. Type: dataset. [1](#)
- [62] Xiu-Shen Wei, Yi-Zhe Song, Oisin Mac Aodha, Jianxin Wu, Yuxin Peng, Jinhui Tang, Jian Yang, and Serge Belongie. Fine-Grained Image Analysis with Deep Learning: A Survey. *IEEE Transactions on Pattern Analysis and Machine Intelligence*, pages 1–1, 2021. Conference Name: IEEE Transactions on Pattern Analysis and Machine Intelligence. [1](#)
- [63] Xiu-Shen Wei, Chen-Wei Xie, Jianxin Wu, and Chunhua Shen. Mask-CNN: Localizing parts and selecting descriptors for fine-grained bird species categorization. *Pattern Recognition*, 76:704–714, Apr. 2018. [2](#)
- [64] Qin Xu, Jiahui Wang, Bo Jiang, and Bin Luo. Fine-Grained Visual Classification via Internal Ensemble Learning Transformer. *IEEE Transactions on Multimedia*, 25:9015–9028, 2023. Conference Name: IEEE Transactions on Multimedia. [6](#)
- [65] Shaokang Yang, Shuai Liu, Cheng Yang, and Changhu Wang. Re-rank Coarse Classification with Local Region Enhanced Features for Fine-Grained Image Recognition, Feb. 2021. arXiv:2102.09875 [cs]. [3](#)
- [66] Ze Yang, Tiange Luo, Dong Wang, Zhiqiang Hu, Jun Gao, and Liwei Wang. Learning to Navigate for Fine-Grained Classification. In Vittorio Ferrari, Martial Hebert, Cristian Sminchisescu, and Yair Weiss, editors, *Computer Vision – ECCV 2018*, Lecture Notes in Computer Science, pages 438–454, Cham, 2018. Springer International Publishing. [1](#), [2](#)
- [67] Shuo Ye, Yu Wang, Qinmu Peng, Xinge You, and C. L. Philip Chen. The Image Data and Backbone in Weakly Supervised Fine-Grained Visual Categorization: A Revisit and Further Thinking. *IEEE Transactions on Circuits and Systems for Video Technology*, 34(1):2–16, Jan. 2024. Conference Name: IEEE Transactions on Circuits and Systems for Video Technology. [6](#), [13](#)
- [68] Shuo Ye, Shujian Yu, Yu Wang, and Xinge You. R2-trans: Fine-grained visual categorization with redundancy reduction. *Image and Vision Computing*, 143:104923, Mar. 2024. [6](#)
- [69] Lianbo Zhang, Shaoli Huang, Wei Liu, and Dacheng Tao. Learning a Mixture of Granularity-Specific Experts for Fine-Grained Categorization. In *2019 IEEE/CVF International Conference on Computer Vision (ICCV)*, pages 8330–8339, Seoul, Korea (South), Oct. 2019. IEEE. [6](#)
- [70] Ning Zhang, Jeff Donahue, Ross Girshick, and Trevor Darrell. Part-Based R-CNNs for Fine-Grained Category Detection. In David Fleet, Tomas Pajdla, Bernt Schiele, and Tinne Tuytelaars, editors, *Computer Vision – ECCV 2014*, Lecture Notes in Computer Science, pages 834–849, Cham, 2014. Springer International Publishing. [2](#)
- [71] Yuan Zhang, Jian Cao, Ling Zhang, Xiangcheng Liu, Zhiyi Wang, Feng Ling, and Weiqian Chen. A free lunch from ViT:

- adaptive attention multi-scale fusion Transformer for fine-grained visual recognition. In *ICASSP 2022 - 2022 IEEE International Conference on Acoustics, Speech and Signal Processing (ICASSP)*, pages 3234–3238, May 2022. ISSN: 2379-190X. [1](#), [2](#), [6](#), [14](#)
- [72] Chuanxia Zheng, Tat-Jen Cham, and Jianfei Cai. The Spatially-Correlative Loss for Various Image Translation Tasks. In *2021 IEEE/CVF Conference on Computer Vision and Pattern Recognition (CVPR)*, pages 16402–16412, Nashville, TN, USA, June 2021. IEEE. [3](#)
- [73] Heliang Zheng, Jianlong Fu, Zheng-Jun Zha, and Jiebo Luo. Looking for the Devil in the Details: Learning Trilinear Attention Sampling Network for Fine-Grained Image Recognition. In *2019 IEEE/CVF Conference on Computer Vision and Pattern Recognition (CVPR)*, pages 5007–5016, Long Beach, CA, USA, June 2019. IEEE. [6](#)
- [74] Zhun Zhong, Liang Zheng, Guoliang Kang, Shaozi Li, and Yi Yang. Random Erasing Data Augmentation. *Proceedings of the AAAI Conference on Artificial Intelligence*, 34(07):13001–13008, Apr. 2020. Number: 07. [6](#), [14](#), [15](#)
- [75] Haowei Zhu, Wenjing Ke, Dong Li, Ji Liu, Lu Tian, and Yi Shan. Dual Cross-Attention Learning for Fine-Grained Visual Categorization and Object Re-Identification. In *2022 IEEE/CVF Conference on Computer Vision and Pattern Recognition (CVPR)*, pages 4682–4692, June 2022. ISSN: 2575-7075. [1](#), [2](#), [3](#), [8](#), [14](#)
- [76] Peiqin Zhuang, Yali Wang, and Yu Qiao. Learning Attentive Pairwise Interaction for Fine-Grained Classification. *Proceedings of the AAAI Conference on Artificial Intelligence*, 34(07):13130–13137, Apr. 2020. Number: 07. [1](#), [6](#)

## Appendix for Global-Local Similarity for Efficient Fine-Grained Image Recognition with Vision Transformers

### A. Extended Comparison of ViTs for FGIR

We summarize the differences between various ViT models proposed for FGIR in Table 6. The following aspects are considered: (i) Patch Overlap (PO), which indicates whether the ViT’s patchifier convolution has overlapping stride; (ii) Intermediate Features (IF), which refers to whether the model uses intermediate values (features or attention scores); (iii) Discriminative Feature Selection Mechanism (DFSM), which describes how the model selects discriminative features; (iv) Crops, which indicates whether the model crops the image for a second forward pass; (v) Feature Aggregation (FA), which denotes the modules used for performing discriminative feature refinement or aggregation; and (vii) Complexity. The ‘✓’ represents the model uses the feature, while ‘-’ represents it was not.

We observe that 1) many of the proposed modifications to the original ViT are modular and can be substituted or combined and 2) the most significant difference between these methods lies in their DFSM. For this reason, we focus on this aspect in Table 1 in the main text, and Tables 7 and 8 in the Appendix.

We note how the cubic complexity of matrix-multiplication based attention aggregation mechanisms is pervasive across architectures with different patch size (see Table 7) and model capacity (Table 8). Furthermore, the percentage of computation required by these mechanisms increases as the patch size or model capacity decreases. This can hinder the applicability of attention rollout and similar mechanisms in resource constrained environments.

### B. Pseudocode for Our Method

We include Pytorch-like pseudocode to facilitate the understanding of our method, noting the tensor dimensions at the different steps of the forward pass, in Figure 6.

### C. Extended Experimental Setup

Previous research suggested the applicability of FGIR methods is task dependent [67]. Therefore, to obtain a better understanding of how our method performs across FGIR tasks we conduct a comparison across 10 diverse FGIR datasets. The statistics for the evaluated datasets are shown in Table 9.

The training and test settings employed in our experiments are summarized in Table 10. For each model and dataset pair, we first perform a learning rate (LR) search with a training and validation set created by partitioning 80% and 20% of the total training data (train-val), respectively. However, for datasets with more than 50,000 im-

```
def gls(feats, images):
    # global representation (CLS token, first one)
    # local representations (other patches)
    global_rep = feats[:, :1, :]
    local_rep = feats[:, 1:, :]

    # our proposed metric: GLS
    # cosine similarity between global-local
    sim = cosine_sim(global_rep, local_rep, dim=-1)

    # crop based on top-0 highest values of GLS
    crops = crop_images(sim, images)
    return crops

def forward(self, images):
    # images: tensor w/ shape B, C, H, W
    # B: batch size, C: input channels
    # H: height, W: width

    # extract features using ViT encoder
    feats = self.encoder(images)
    # feats shape: B, N, D
    # N: sequence length (spatial dimension)
    # D: transformer hidden dim size

    # crop based on proposed global-local similarity
    crops = gls(feats, images)

    # extract features for crops (same encoder)
    feats_crops = self.encoder(crops)

    # concat CLS token of original and crops
    cls = feats[:, :1]
    cls_crops = feats_crops[:, :1]
    x = torch.cat([cls, cls_crops], dim=1)
    # x shape: B, 2, D

    # aggregate features from original and crop
    x = self.aggregator(x)

    # first token as input to classifier for preds
    preds = self.head(x[:, 0])
    # preds shape: B, K with K = number of classes
    return preds
```

Figure 6. Pytorch-like pseudocode for the forward pass of GLSim.

ages in the train-val set (DAFB, Food, iNat17), we set the partition ratio to 20% and 80%. We subsequently train the models on the entire training-validation set, using three different seeds (1, 10, 100) each, except for the larger datasets mentioned earlier, where we only employ two seeds (1, 10). The models are trained for 50 epochs, except for the CAL model, which is trained for 160 epochs as per the original author’s recommendation, except for DAFB, Food, and iNat17, where we train for 50 epochs.

We employ the SGD optimizer with batch size of 8, weight decay of 0 (except for CAL, where it is set to  $5 \times 10^{-4}$ ), and cosine annealing [35] with a warmup of 500 steps (1,500 for CAL) for learning rate scheduling.

Regarding the preprocessing of images, we first normalize them and then resize them to a square of size  $1.34S_1 \times 1.34S_2$ . We then perform a random crop during training and a center crop during inference.

In addition to the application of random horizontal flip-

Model	PO	IF	DFSM	Crops	FA	Complexity
TransFG [18]	✓	✓	PSM	-	Transformer	$L \cdot H \cdot N^3$
FFVT [59]	-	✓	MAWS	-	Transformer	$L \cdot H \cdot N$
RAMS-Trans [22]	-	✓	Rollout	✓	-	$L \cdot N^3$
AF-Trans [71]	✓	✓	SACM	✓	-	$L \cdot H \cdot N^2$
DCAL [75]	-	✓	Rollout	-	X-Attention	$L \cdot N^3$
Ours	-	-	GLS	✓	Transformer	$N \cdot D$

Table 6. Summary of differences between ViTs for FGIR.

Model	TransFG [18]	Various [22, 34, 75]	FFVT [59]	AF-Trans [22]	Ours
DFSM	PSM	Rollout	MAWS	SACM	GLS
Complexity	$L \cdot H \cdot N^3$	$L \cdot N^3$	$L \cdot H \cdot N$	$L \cdot H \cdot N^2$	$N \cdot D$
FLOPs (IS=224)	$2.7 \times 10^4$	$3.8 \times 10^2$	$1.7 \times 10^{-1}$	$3.1 \times 10^1$	$5.9 \times 10^{-1}$
% of Backbone	<b>117.51</b>	1.6455	0.0007	0.1344	0.0025
FLOPs (IS=448)	$1.7 \times 10^6$	$2.4 \times 10^4$	$6.9 \times 10^{-1}$	$5.0 \times 10^2$	$2.4 \times 10^0$
% of Backbone	<b>1624.4</b>	22.212	0.0006	0.4649	0.0022
FLOPs (IS=768)	$4.6 \times 10^7$	$5.5 \times 10^5$	$2.0 \times 10^0$	$4.4 \times 10^3$	$6.7 \times 10^0$
% of Backbone	<b>11362</b>	<b>134.39</b>	0.0005	1.09	0.0017
FLOPs (IS=1024)	$2.7 \times 10^8$	$3.3 \times 10^6$	$3.6 \times 10^0$	$1.4 \times 10^4$	$1.2 \times 10^1$
% of Backbone	<b>27554</b>	<b>339.94</b>	0.0004	1.4676	0.0013

Table 7. Summary of computational cost for discriminative feature selection mechanisms (DFSM) used by ViTs in FGIR and their ratio of FLOPs compared to the backbone for ViT B-14. We highlight in **bold** values that exceed 50% of the FLOPs of the backbone.

Model	TransFG [18]	Various [22, 34, 75]	FFVT [59]	AF-Trans [22]	Ours
DFSM	PSM	Rollout	MAWS	SACM	GLS
Complexity	$L \cdot H \cdot N^3$	$L \cdot N^3$	$L \cdot H \cdot N$	$L \cdot H \cdot N^2$	$N \cdot D$
FLOPs (IS=224)	$2.1 \times 10^3$	$1.7 \times 10^2$	$3.5 \times 10^{-2}$	$2.6 \times 10^0$	$1.1 \times 10^{-1}$
% of Backbone	<b>160.36</b>	13.228	0.0027	0.2062	0.0089
FLOPs (IS=448)	$1.5 \times 10^5$	$1.1 \times 10^4$	$1.4 \times 10^{-1}$	$4.7 \times 10^1$	$4.5 \times 10^{-1}$
% of Backbone	<b>2130.8</b>	<b>147.35</b>	0.0019	0.6485	0.0063
FLOPs (IS=768)	$3.8 \times 10^6$	$2.7 \times 10^5$	$4.1 \times 10^{-1}$	$3.9 \times 10^2$	$1.3 \times 10^0$
% of Backbone	<b>10037</b>	<b>720.95</b>	0.0011	1.0537	0.0036
FLOPs (IS=1024)	$2.3 \times 10^7$	$1.5 \times 10^6$	$7.2 \times 10^{-1}$	$1.3 \times 10^3$	$2.4 \times 10^0$
% of Backbone	<b>22568</b>	<b>1509.0</b>	0.0007	1.3015	0.0024

Table 8. Summary of computational cost for discriminative feature selection mechanisms (DFSM) used by ViTs in FGIR and their ratio of FLOPs compared to the backbone for ViT T-16. We highlight in **bold** values that exceed 50% of the FLOPs of the backbone.

ping during training, we further incorporate a stronger set of augmentation and regularization (AugReg) techniques that have been shown to improve the generalization capabilities of models and mitigate overfitting. Our choice of AugReg is motivated by recent advances in training strategies for coarse image recognition [53, 54]. Specifically, random erasing [74] and trivial augment [38] are employed for the purpose of data augmentation. For regularization, we employ label smoothing [52] and stochastic depth [23], albeit

the latter only for ViT-based models.

## D. Extended Results and Discussion

### D.1. Extended Analysis on Computational Cost

We compare the trade-off between accuracy and the throughput (in images per second) at inference time when batching the images, and the associated VRAM (in Gigabytes) required for computing this batched inference. For

Dataset	$T$	# Train	# Test	$\overline{S}_1$	$\overline{S}_2$
CUB [58]	200	5,994	5,794	468	386
DAFB [7, 47]	3,263	368,997	94,440	268	340
Dogs [27]	120	12,000	8,580	443	386
Flowers [39]	102	2,040	6,149	623	536
Food [6]	101	75,750	25,250	496	475
iNat17 [56]	5,089	579,184	95,986	746	645
Moe [1]	173	11,454	2,943	159	146
NABirds [55]	600	23,929	24,633	901	713
Pets [41]	37	3,680	3,669	431	383
VegFru [20]	292	43,800	116,391	347	287

Table 9. Statistics for evaluated datasets.  $T$ ,  $\overline{S}_1$  and  $\overline{S}_2$  Represent number of classes, average width and height, respectively.

Setting	Value
Models	{ResNet-101 [19], CAL [44], ViT B-16 [12], TransFG [18], FFVT [59], GLSim}
Optimizer	SGD
LR range	{0.03, 0.01, 0.003, 0.001}
Batch size	8
Weight decay	0*
Epochs	50*
LR Schedule	Cosine with Warmup for 500* Steps
Image size	{224, 448}
Preprocess	Normalize then square resize followed by random (train) or center (inference) crop
Augmentations	Random Horizontal Flip, Random Erasing [74], Trivial Augment [38]
Regularization	Label Smoothing [52], Stochastic Depth [23]

Table 10. Training (and Inference) Hyperparameter Settings. \*With exceptions for CAL. Details are described in Appendix C.

the batched throughput we first compare the throughput at different batch sizes, from 1 to 256 for all these model-image size pairs, and select the batch size which led to the highest throughput (and corresponding VRAM requirements).

In Figure 4 of the main text we show the results on accuracy vs inference throughput. We additionally show the results on Figure 7 on accuracy vs inference memory re-

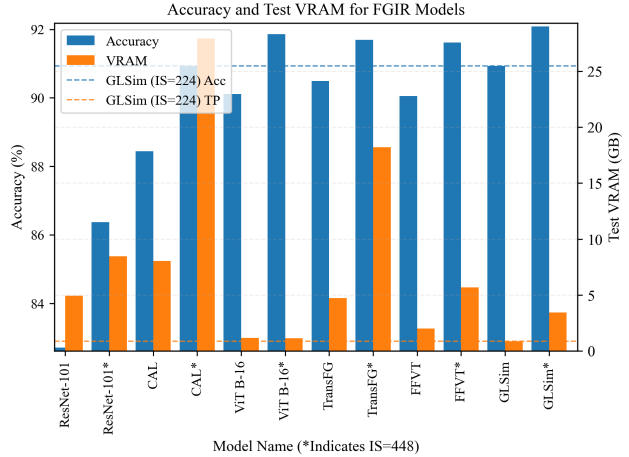


Figure 7. Accuracy and VRAM plots for the evaluated models on CUB. *Model\** represents results for image size 448x448.

quirements as the VRAM requirement is also an important decision when deploying models. Discussion is included in Section 5.3 of the main text.

## D.2. Effects of Augmentation and Regularization on FGIR

While the impact of generic Augmentations and Regularizations (AugReg) on coarse image recognition has been widely studied, its influence on FGIR has received less attention. In general, newer coarse recognition backbones are trained using strong augmentations and regularization techniques, such as Random Erasing (RE) [74], AutoAugment (AA) [9], TrivialAugment (TA) [38] Label Smoothing (LS) [52], and Stochastic Depth (SD) [23]. However, in FGIR, works typically only incorporate random cropping (RC) and random horizontal flipping (RF), with some newer works [18, 59] also using LS.

The reasoning behind this is that strong augmentations may obfuscate the subtle differences required to distinguish between fine-grained categories. As a result, a line of FGIR research has emerged, focused on designing data-aware AugReg techniques. One prominent work in this area is WS-DAN [21], which proposes using attention maps to guide cropping and masking of a given image during training. These two techniques are employed in alternation throughout the training process to both augment the input images the network processes and regularize the network, preventing overfitting. Furthermore, during inference multiple crops are obtained to maximize recognition performance. CAL [44] builds on WS-DAN by using counterfactual causality to measure the attention quality and guide this process. However, as seen in Figure 4 in the main text this process incurs considerable computational cost during inference.

Model	Minimal (RC + RF)	Weak (++LS)	Medium (++SD)	Strong (++RE + TA)
ResNet-101	80.85 ± 0.62	<u>81.03 ± 0.29</u>	80.89 ± 0.55	<b>82.71 ± 0.06</b>
CAL	86.39 ± 0.89	87.01 ± 0.12	<u>87.36 ± 0.28</u>	<b>88.44 ± 0.25</b>
ViT B-16	88.27 ± 0.2	88.53 ± 0.27	<u>89.5 ± 0.21</u>	<b>90.11 ± 0.17</b>
TransFG	89.06 ± 0.23	88.94 ± 0.16	<u>89.93 ± 0.24</u>	<b>90.49 ± 0.06</b>
FFVT	88.83 ± 0.04	88.78 ± 0.09	<b>90.15 ± 0.2</b>	<u>90.05 ± 0.04</u>
GLSim	89.78 ± 0.13	89.72 ± 0.38	<u>90.49 ± 0.26</u>	<b>90.93 ± 0.24</b>
ResNet-101*	84.72 ± 0.25	85.16 ± 0.39	<u>85.25 ± 0.45</u>	<b>86.37 ± 0.22</b>
CAL*	89.39 ± 0.11	<u>88.9 ± 0.48</u>	87.61 ± 1.53	<b>90.94 ± 0.21</b>
ViT B-16*	90.13 ± 0.13	90.51 ± 0.17	<u>91.44 ± 0.14</u>	<b>91.86 ± 0.01</b>
TransFG*	90.6 ± 0.11	90.31 ± 0.07	<u>91.25 ± 0.02</u>	<b>91.69 ± 0.15</b>
FFVT*	90.1 ± 0.22	90.05 ± 0.08	<b>91.69 ± 0.1</b>	<u>91.61 ± 0.04</u>
GLSim*	91.06 ± 0.08	91.1 ± 0.19	<u>91.89 ± 0.14</u>	<b>92.09 ± 0.01</b>

Table 11. Effects of Augmentations and Regularization (AugReg) on Fine-Grained Recognition Accuracy for CUB Dataset. ++ Represents All Previous AugReg are Used. RC, RF, LS, SD, RE, and TA stand for Random Crop, Random Horizontal Flip, Label Smoothing, Stochastic Depth, Random Erase, and Trivial Augment, Respectively. Best and Second Best AugReg Settings For Each Model are Highlighted in **Bold** and Underline, Respectively. *Model\** Represents Results For Image Size 448.

Therefore, we explore the potential behind incorporating generic AugReg techniques developed for coarse image recognition into FGIR tasks. Specifically, we compare four different levels of AugReg: minimal, weak, medium, and strong. The minimal level only employs RC and RF, and is the setting most commonly used in FGIR works [21, 44]. The weak level, which is used in newer works [18, 59], also applies LS. The medium level further incorporates SD with a probability of 0.1. Finally, the strong level additionally includes RE and TA. We select TA based on qualitative evaluation that indicates its application of less severe distortions to the image compared to AA. The effects of AugReg choice on classification accuracy for the CUB dataset are shown in Table 11.

We observe that AugReg is indeed a crucial factor for FGIR and can have a significant impact on accuracy, often rivaling the effect of image size and the choice of model. On the CUB dataset, we observe an average absolute accuracy improvement of 1.59% and 1.43% for image sizes of 224x224 and 448x448, respectively, when using strong AugReg compared to minimal AugReg. For reference, the average absolute accuracy improvement from increasing the image size from 224 to 448 on the CUB dataset is 1.97%.

Since incorporating stronger AugReg incurs minimal increase in training cost while not increasing inference cost at all we suggest practitioners to consider stronger generic AugReg as a cost-efficient method to improve recognition performance.

### D.3. Extended Ablations

#### D.3.1 Importance of Aggregator for Crop Robustness

To demonstrate the importance of the Aggregator module to our system, we conduct an ablation utilizing crops obtained via random selection. Results are shown in Table 12. As seen in the second row, incorporating random crops without the Aggregator module results in a decrease in performance compared to the baseline, as the random crops deteriorate the quality of input data. Through the usage of our Aggregator module, the method obtains robustness to incorporating random crops, as the self-attention mechanism allows for dynamic reweighting of the contribution of the crops vs the original image. Therefore, when the crops are sub-optimal, the model can effectively discard noise and contributions from the crops.

On the other side, when we guide the crop selection through the proposed GLS metric and the quality of the crop improves, the Aggregator modules incorporates this information to decrease the classification error by 8.29%. These results, along with the ones presented in Section 5.4 illustrate the importance of both the GLS module for discriminative feature selection and the Aggregator module for high-level feature refinement.

#### D.3.2 Hyperparameter $O$

We investigate the impact of the hyperparameter  $O$ , which governs how many tokens with the highest similarity are employed for crop selection, on the classification performance, in Table 13. Smaller values lead to more aggressive cropping that may fail to crop the object of interest,

Baseline (ViT B-16)	90.11 $\pm$ 0.24
Random Crops W/O Aggregator	89.47 $\pm$ 0.19
Random Crops With Aggregator	90.26 $\pm$ 0.27
GLSim With GLS Crops	<b>90.93 <math>\pm</math> 0.24</b>

Table 12. Ablation on importance of Aggregator module for robustness to non-optimal crops.

while higher values may return a high percentage of background. Despite this, the findings indicate that the proposed approach is relatively robust to variations in this selection criterion, as all improve upon the baseline by at least 5.87% in the case of  $O = 4$  and up to 8.29% in the case of  $O = 8$ .

4	8	16	32
90.69 $\pm$ 0.25	<b>90.93 <math>\pm</math> 0.24</b>	90.85 $\pm$ 0.17	90.82 $\pm$ 0.30

Table 13. Ablation on  $O$  hyperparameter for cropping on CUB.

### D.3.3 Similarity Metric

We study the effects of similarity metric choice in Table 14. We were inspired to employ cosine similarity due to its relation to self-attention, both involving dot products, but these results show that our method exhibits robustness to the metric selection, as all reduce the ViT baseline relative classification error by at least 8.63%.

Cosine	L1	L2
90.93 $\pm$ 0.24	<b>91.03 <math>\pm</math> 0.21</b>	90.93 $\pm$ 0.13

Table 14. Ablation on similarity metric for selecting crops on CUB.

### D.3.4 Vision Transformer’s Patch Size

We evaluated the proposed system using two distinct patch sizes in Table 15. It is worth remarking that the kernel and stride size utilized in the ViT’s patchifier are critical factors that directly influence the granularity of the feature maps, albeit at the expense of increased computational overhead, resulting from the greater effective sequence length.

Results show that the relative classification error compared to the baseline can be reduced by up to 17.23% for the model with patch size 32. These demonstrate the efficacy of the proposed approach at various feature map granularities.

Patch Size	Baseline (Vanilla ViT)	GLSim
16	90.11 $\pm$ 0.24	<b>90.93 <math>\pm</math> 0.17</b>
32	85.84 $\pm$ 0.17	<b>88.28 <math>\pm</math> 0.02</b>

Table 15. Ablation on vision transformer patch size on CUB.

## E. Additional Samples on GLS For Visualization

We include additional samples of the proposed GLS metric as a visualization tool to highlight which local regions of the image have high similarity to the global representation from the CLS token to interpret classification predictions when combined with state-of-the-art pretrained backbones DINOv2 B-14 [40] across different datasets in Figure 8 to Figure 14.



Figure 8. Visualization of attention-based visualization mechanisms and our proposed GLS for DINOv2 B-14 [40] on CUB.

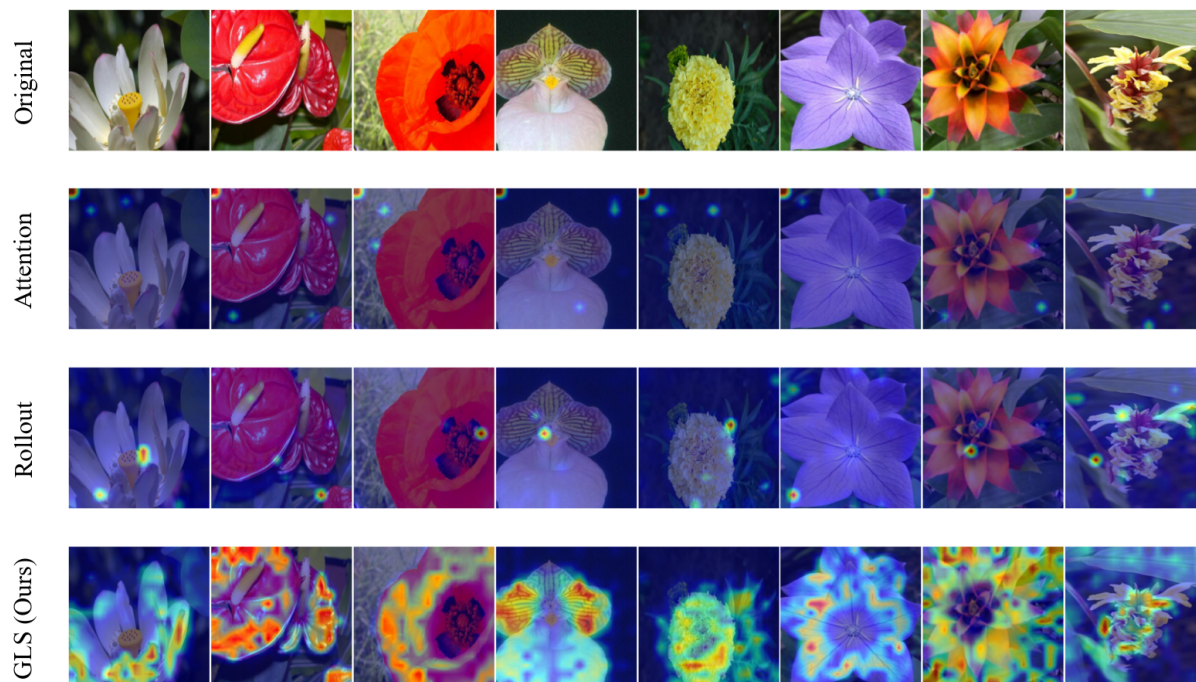


Figure 9. Visualization of attention-based visualization mechanisms and our proposed GLS for DINOv2 B-14 [40] on Flowers.

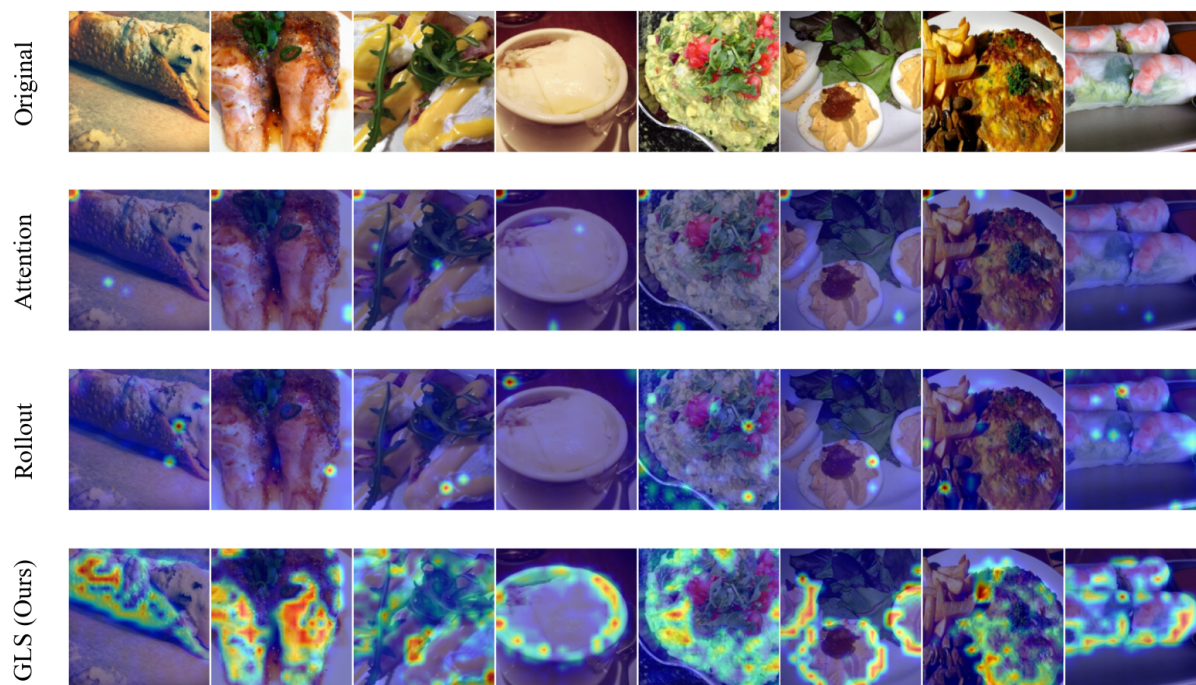


Figure 10. Visualization of attention-based visualization mechanisms and our proposed GLS for DINOv2 B-14 [40] on Food.

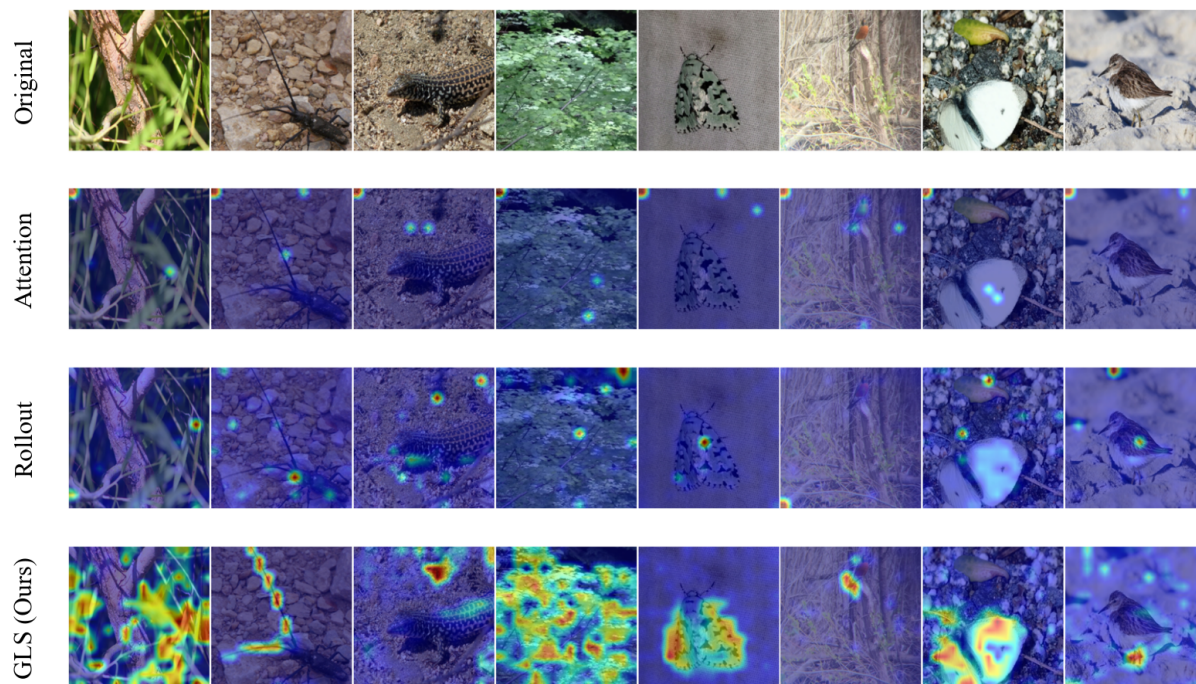


Figure 11. Visualization of attention-based visualization mechanisms and our proposed GLS for DINOv2 B-14 [40] on iNat17.

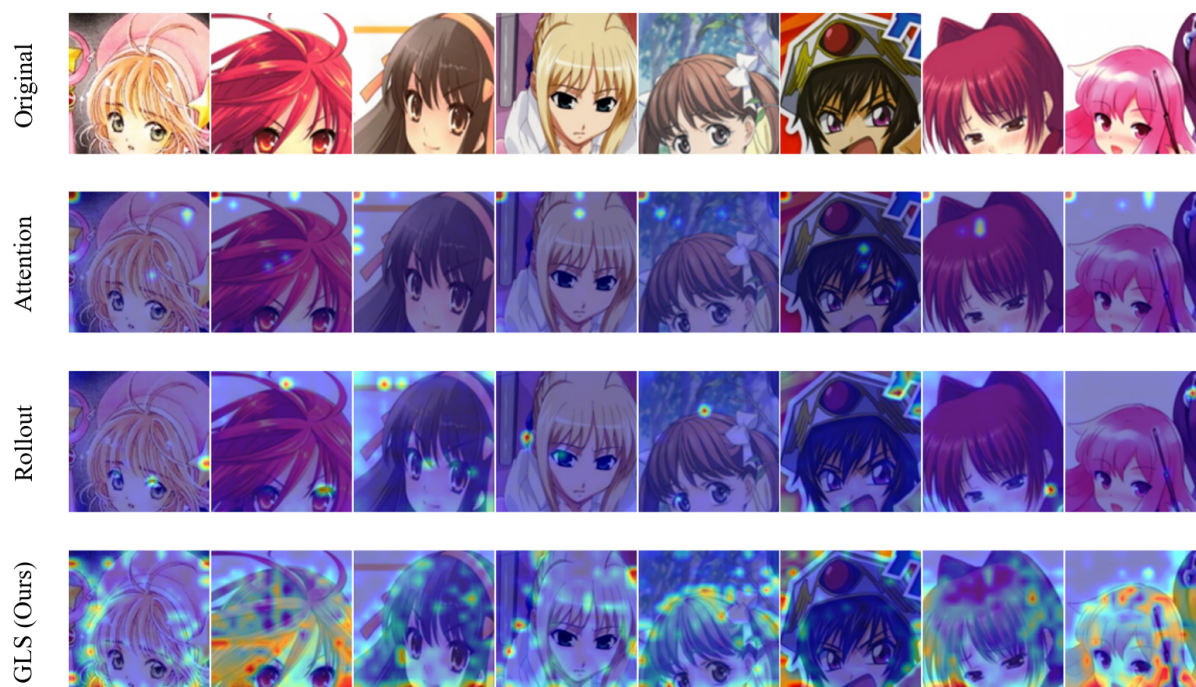


Figure 12. Visualization of attention-based visualization mechanisms and our proposed GLS for DINOv2 B-14 [40] on Moe.



Figure 13. Visualization of attention-based visualization mechanisms and our proposed GLS for DINOv2 B-14 [40] on Pets.



Figure 14. Visualization of attention-based visualization mechanisms and our proposed GLS for DINOv2 B-14 [40] on VegFru.